Chen, Q. and Srebric, J. 2000. "Application of CFD tools for indoor and outdoor environment design," Invited paper, *International Journal on Architectural Science*, 1(1), 14-29.

Application of CFD Tools for Indoor and Outdoor Environment Design

Qingyan Chen and Jelena Srebric
Building Technology Program, Department of Architecture,
Massachusetts Institute of Technology,
77 Massachusetts Avenue, Cambridge, MA 02139-4307, U.S.A.
Phone: (617) 253-7714, Fax: (617) 253-6152, Email: qchen@mit.edu

Abstract

Computational Fluid Dynamics (CFD) has become a useful tool for the study of indoor and outdoor environment problems. Recently, the Massachusetts Institute of Technology (MIT) has developed several Reynolds Averaged Navier-Stokes (RANS) equation models and Large Eddy Simulation (LES) models to enhance the capabilities of CFD for use in indoor and outdoor environment design. The new models have been successfully used to assess building shape design, to evaluate the effectiveness of natural ventilation in buildings, to model Volatile-Organic-Compound (VOC) emissions from building materials, and to calculate indoor environment parameters.

Nomenclature

Ar	Archimedes number
Ar_y	local Archimedes number, $g\beta\Delta Ty_n / U^2$
C	contaminant concentration
C	coefficient for subgrid scale model ($C=Cs^2$)
$C_{1\varepsilon}$, $C_{2\varepsilon}$, $C_{3\varepsilon}$	constants used in the ε equation
C_m	VOC concentration in the solid material
Cs	Smagorinsky model coefficient
C_μ	constant used for calculating ν_t
D	room depth
D_m	diffusion coefficient of the VOC in the solid material
d_k	diffusion of turbulent kinetic energy
$E_{ij}(C)$	integrated square of the error function
e_{ij}	error function for C
$f_{l\mu}$, $f_{l\varepsilon}$, f_{vv}	functions used in the one-equation model
$G(x_i)$	filter function
$\widetilde{G}$	test filter
$\overline{G}$	grid filter
$G_f(\mathbf{x},\mathbf{x}')$	smooth function over **x**
G_k	gravity production of turbulent kinetic energy, $-\beta g_i \overline{u_i t}$
g_i	component i of the gravitation vector
H	room height
h	height

K_{ma}	dimensionless material-air partition coefficient.
k	turbulent kinetic energy, $\overline{u_i u_i}/2$
L	room width
L_{ij}	$L_{ij} = \widetilde{\bar{u}_i \bar{u}_j} - \widetilde{\bar{u}}_i \widetilde{\bar{u}}_j$
l, l_μ, l_ε	characteristic lengths
P_k	shear production of the turbulent kinetic energy, $-\overline{u_i u_j}\,\partial U_i/\partial x_j$
Pr_t	turbulent Prandtl number
$\bar{p}_i$	grid filtered pressure
Ra	Rayleigh number
Re	Reynolds number
S_Φ	source term for Φ
T	mean temperature
T_f	floor temperature
T_{ij}	turbulent stress on the test filter
t	time
U_i, U_j	component i and j of the mean velocity
U, V, W	mean velocity component in the x, y and z direction
u, v	fluctuating velocity component in the x, y direction
u_i, u_j	velocity component in x_i and x_j direction
$\bar{u}_i$, $\bar{u}_j$	grid filtered velocity component in x_i and x_j direction
$\widetilde{\bar{u}}_i$	test filtered velocities
x_i, x_j	spatial coordinate in the i and j direction
x, y, z	spatial coordinate
y_n	normal distance to the nearest wall
y^*	dimensionless wall distance, $y_n\sqrt{k}/\nu$

Greek symbols

β	thermal expansion coefficient
Γ_Φ	effective diffusion coefficient for Φ
Δ	filter size
$\widetilde{\Delta}$	test filter size
$\overline{\Delta}$	grid filter size
ε	turbulent energy dissipation
ν	kinematic viscocity
ν_t	turbulent viscocity
ρ	air density
σ_k, σ_ε	Prandtl number of k and ε
τ_{ij}	time
Φ	= 1 for mass continuity
Φ	= u_j (j = 1, 2, and 3) for three components of momentum (u,v,w)
Φ	= T for temperature

Φ = C for concentrations

Subscripts

i, j	spatial coordinate indices
in	inlet
t	turbulent quantities

Introduction

The CFD technique has become a tool for predicting engineering flows since the early 1970s, due to the development in computer programming and turbulence models. CFD solves fluid flow, heat transfer, and chemical species transport. The parameters solved, such as air velocity, air temperature, contaminant concentrations, relative humidity, and turbulence quantities, are crucial for designing a comfortable indoor or outdoor environment. This is because the design of appropriate ventilation systems and the development of control strategies require detailed knowledge of airflow, contaminant dispersion and temperature distribution in a building. This knowledge is also required by architects for designing the building configuration. In the past thirty years, the CFD technique has been applied with considerable success in building design, as reviewed by Chen (1997) and Murakami (1998).

The CFD approaches are normally classified into three types: Direct Numerical Simulation (DNS), Reynolds Averaged Navier-Stokes (RANS) equation modeling, and Large Eddy Simulation (LES).

DNS solves the highly reliable Navier-Stokes equations without approximations. Therefore, DNS requires a grid resolution as fine as the Kolmogorov micro-scale. Since the Reynolds number is approximately 10^6 for typical wind flow and approximately 10^5 for indoor airflow, the total grid number for solving airflow in and around a building is approximately 10^{13}. Current super computers can have a grid resolution as fine as 512^3. The computer capacity is still far too small to solve such a flow. Therefore, DNS cannot be used to study indoor and outdoor environment under a realistic condition.

RANS solves ensemble-averaged Navier-Stokes equations by using turbulence modeling. RANS can be further divided into turbulent viscosity models and Reynolds-stress models. The most widely used turbulent viscosity model is the standard k-ε model (Launder and Spalding 1974). Chen (1995) compared five different k-ε models for the prediction of natural, forced, and mixed convection in rooms, as well as an impinging jet flow. These models failed to predict the anisotropic turbulence and secondary recirculation of indoor airflow. The Reynolds-stress models solve the transport equations for the Reynolds stresses. Recent effort on the Reynolds-stress models focuses on how to improve the pressure-strain correlation. Murakami (1993) used four different Reynolds-stress models to calculate the reattachment lengths around a cube. All the models significantly over-predicted (40% to 90%) the lengths. Chen (1996) used three different Reynolds-stress model to predict indoor airflows with natural, forced, and mixed convection. The performance of those models was not much better than the standard k-ε model. In addition, the models are mathematically complex and numerically unstable.

LES was developed in the early 1970s by Deardorff (1970) for meteorological applications. He departed from the hypothesis that the turbulent motion could be separated into large-eddies and small-eddies. The separation between the two does not have a significant effect

on the evolution of large-eddies. LES solves the large-eddy motion by a set of filtered equations governing the three-dimensional, time dependent motion. Turbulent transport approximations are used for small eddies which are modeled independently from the flow geometry. The success of LES stems from the fact that the main contribution to turbulent transport comes from the large-eddy motion. Thus, LES is clearly superior to RANS where the transport terms (e.g. Reynolds stresses) are treated with full empiricism. LES is also more realistic than DNS because LES can be performed on a large and fast workstation.

Murakami (1998) reviewed the use of LES for airflow around buildings. He found that LES gave the best accuracy and the standard k-ε model the worst. Very few applications of LES are for indoor airflow. These applications include the prediction of forced convection in an empty room (Davidson and Nielsen 1996 and 1998, Emmerich and McGrattan 1998, and Zhang and Chen 2000). The results show that LES can predict indoor airflow, especially the turbulence level, more accurately than RANS.

At present, LES needs at least 512 megabytes of computer memory to separately study indoor airflow or outdoor airflow only. For natural ventilation where indoor and outdoor airflow must be studied simultaneously, LES would require several gigabytes of computer memory. Since LES simulates airflow in a three-dimensional, time-dependent manner, the computing time needed is much longer than that by RANS. With a 533 MHz Alpha workstation, a typical run with LES is two to three days, while with RANS it is only two to three hours for indoor airflow simulation. Although the computing costs seem to be high at present, the fast development in computing power will make LES an affordable design tool in the near future.

This paper will demonstrate some efforts at the Massachusetts Institute of Technology (MIT) to use CFD as a design tool for indoor and outdoor environment design.

RANS Model Development

Based on the review above, the effort at MIT in the past few years has been to use RANS as a main design tool and to use LES as an advanced tool. For an incompressible and Newtonian flow, the RANS conservation equations for continuity, momentum (using Boussenisseq approximation for buoyancy), turbulence quantities, energy, and chemical species can be generalized as:

$$\frac{\partial}{\partial t}(\rho\Phi) + \frac{\partial}{\partial x_j}(\rho U_j \Phi) = \frac{\partial}{\partial x_j}(\Gamma_\phi \frac{\partial \Phi}{\partial x_j}) + S_\phi \qquad (1)$$

The Φ, Γ_ϕ and S_ϕ for different flows are shown in Table 1, where the standard k-ε model (Launder and Spalding 1974) is used.

A two-layer k-ε model

Previous studies (Chen 1995 and 1996) found that the Reynolds-stress models and low-Reynolds-number models did not perform much better than the standard k-ε model or the Re-Normalization Group (RNG) k-ε model but were more demanding on computing time. Therefore, the standard k-ε model and the RNG k-ε model have been used for these studies. However, the standard k-ε model and the RNG k-ε model cannot accurately calculate the heat

transfer near a wall. The data from a direct numerical simulation from Kasagi and Nishimura (1997) has been used to develop a new two-layer model to solve the problem.

A two-layer model consists of two turbulence models. This paper uses a single k-equation turbulence model for near-wall flow and the standard k-ε model for flow in the outer-wall region. The criteria to switch from one model to the other is the y* value. If $y^* < y^*_{prescribed}$, the single-equation model applies; otherwise, the standard k-ε model will be used. $y^*_{prescribed} = 80$ seems optimum for room airflow.

In the near-wall region, where $y^* < 80$, the new one-equation model is used through which k is solved by Eq. (2),

$$\frac{\partial k}{\partial t} + U_i \frac{\partial k}{\partial x_i} = d_k + P_k + G_k - \varepsilon \tag{2}$$

The eddy viscosity is calculated by Eq. (3):

$$\nu_t = \sqrt{\overline{vv}}\, l_\mu \tag{3}$$

and the ε by Eq. (4):

$$\varepsilon = \frac{\sqrt{\overline{vv}}\, k}{l_\varepsilon} \tag{4}$$

Then l_μ, l_ε, and $\frac{\overline{vv}}{k}$ are determined by Eqs. (5), (6) and (7) respectively.

$$l_\mu = \frac{(0.33 + 0.214 f_{l_\mu})y}{1 + 5.025 \times 10^{-4} y_v^{*[1.53 + 0.12 f_{l_\mu}]}} \tag{5}$$

$$l_\varepsilon = \frac{(1.3 + 7.5 f_{l_\varepsilon})y}{1 + \left(2.12 + 7.88 f_{l_\varepsilon}\right)/y_v^* + (0.028 + 0.0235 f_{l_\varepsilon}) y_v^*} \tag{6}$$

$$\frac{\overline{vv}}{k} = 0.4\left[1 - \exp\left(-\frac{y^{*(2 - f_{vv/k})}}{4200(1 - 0.99 f_{vv/k})}\right)\right] \tag{7}$$

where

$$f_{l_\mu} = f_{l_\varepsilon} = \frac{1}{2}\left[1 + \tanh(50 * \left|Ar_y\right| - 4)\right] \tag{8}$$

$$f_{vv/k} = \frac{1}{2}\left[1 + \tanh(120 * \left|Ar_y\right| - 4)\right] \tag{9}$$

In the outer-wall region, where $y^* \geq 80$, the standard k-ε model and Eqs. (10) and (11) are used:

$$\frac{Dk}{Dt} = \frac{\partial}{\partial x_i}\left((\nu + \frac{\nu_t}{\sigma_k})\frac{\partial k}{\partial x_i}\right) + \nu_t(\frac{\partial U_i}{\partial x_j} + \frac{\partial U_j}{\partial x_i}) - \varepsilon + g_i\beta\frac{\nu_t}{Pr_t}\frac{\partial T}{\partial x_i} \quad (10)$$

where σ_k =1.0. The ε is solved by a transport equation

$$\frac{D\varepsilon}{Dt} = \frac{\partial}{\partial x_i}\left((\nu + \frac{\nu_t}{\sigma_\varepsilon})\frac{\partial \varepsilon}{\partial x_i}\right) + \frac{\varepsilon}{k}\left[C_{1\varepsilon}\nu_t(\frac{\partial U_i}{\partial x_j} + \frac{\partial U_j}{\partial x_i}) - C_{2\varepsilon}\varepsilon + C_{3\varepsilon}g_i\beta\frac{\nu_t}{Pr_t}\frac{\partial T}{\partial x_i}\right] \quad (11)$$

The eddy viscosity is calculated by the equation, $\nu_t = C_\mu \frac{k^2}{\varepsilon}$, where C_μ = 0.09. The standard k-ε model does not need a length scale prescription.

This model has been used with success to study forced, natural, and mixed convection flow in a room (Xu 1998). Fig. 1 shows the air velocity and temperature profiles at the center of a simulated office with displacement ventilation. The agreement is very good in the region close to the ceiling. In the region close to the floor, some discrepancies did occur. However, the largest difference between the calculated temperatures and measured ones was less than 1 K, which is about 4% of the measured temperature. This can be considered a good agreement. The numerical simulation conducted by Yuan et al. (1999) used the RNG k-ε model with wall functions to predict the flow and heat transfer. Since wall functions would predict grid dependent heat flux and cause an unacceptable error, a prescribed convective heat transfer coefficient was used to obtain the correct temperature distributions. The value of the coefficient used in their study was calibrated by the experimental data. This is undesirable in a numerical prediction because the coefficient is generally unknown. The two-layer model does not require a prescribed convective heat transfer coefficient, and thus is more favorable for numerical simulations.

The agreement between the numerical results and the measured data is acceptable but not excellent. The models used in the computation may have some uncertainties for indoor airflow prediction due to the assumptions made in the model development. The measurements are also not free from errors. The hot-wire anemometers used in the experiment cannot accurately measure the air velocity when it is lower than 0.1 to 0.15 m/s. Since the velocity level in this case is low, the uncertainty in the measurements of the velocities is rather high.

The grid number required in the current study (52 × 48 × 28) is a little higher than that used by Yuan et al. (1999) (48 × 42 × 24). This study shows that the computing costs with the two-layer model are slightly higher than those with the RNG k-ε model. If the study used a low-Reynolds-number k-ε model, it would require at least one million grid points because there are many heated surfaces in the room. A low-Reynolds-number k-ε model requires at least 20 grid points to correctly calculate the heat transfer from a heated/cooled solid surface. The computing effort would be tremendous.

A zero-equation model

The two-layer model can accurately calculate heat transfer near a wall, while using far less numerical grid points than low-Reynolds-number models. However, the computing time is still too high when simulating transient flow in a room. The simulation of transient flow is important

especially when one would like to understand the thermal comfort and indoor air quality for a few typical days in a building, or obtain wind and pressure information around a building for outdoor comfort and natural ventilation design. A single algebraic function (a zero-equation model) has been developed to express the turbulent viscosity as a function of local mean velocity, V, and a length scale, l:

$$\nu_t = 0.03874\ V\ l \qquad (12)$$

Fig. 1 shows the air velocity and temperature profiles at the center of a simulated office with displacement ventilation. Although the zero-equation model is simple, its performance is as good as that of the two-layer model.

Since no transport equations are solved for turbulence and the equation can lead to a stable solution, the computing time with the zero-equation model is only a fraction of that with the standard k-ε model. Table 2 shows the computing time on a Pentium II PC for an office room with different space layouts and ventilation systems (Fig. 1(a)). Although the grid is coarse, the computing time required is minimal.

The CFD program with the zero-equation model has further been coupled with an energy analysis program. This coupling has the following advantages:

- The CFD program can calculate heat transfer coefficients and air temperature near a wall for use in the energy simulation program.
- The energy simulation program can calculate wall surface temperature and cooling or heating loads as boundary conditions for the CFD program.
- The coupled program can analyze the energy used in a building while providing detailed indoor environment conditions.

Fig. 2(a) shows the heat extraction calculated by the combined program for a typical winter and summer day in a large office with displacement ventilation. The coupled program can also determine the predicted percentage of dissatisfied people due to thermal comfort at three different times of the day (as shown in Fig. 2(b-d)). This calculation uses weather data and building property data as inputs. Therefore, there is no need to provide wall temperatures as boundary conditions for the CFD calculation. Since the CFD program provides accurate heat transfer information in building energy analysis, the results are more accurate. The coupled program exhibits a great potential in indoor environment design.

RANS Model Applications

Recently, RANS models have been applied to study a number of indoor and outdoor environment problems. The following section summarizes a few examples.

Building shape design

Wind is a friend to a building because it can naturally ventilate the building to provide a comfortable and healthy indoor environment as well as to save energy. The conventional design approach often ignores opportunities for innovation that can condition buildings at lower costs or with higher air quality and acceptable thermal comfort level, usually by means of passive cooling or natural ventilation. On the other hand, the wind can be an enemy to the building because it can

cause discomfort to pedestrians if the wind speed around the building is too high. If the air temperature in the winter is low, the chilling effect of the wind could be so strong that pedestrians cannot walk comfortably and safely. Therefore, it is essential to reduce the wind speed around buildings.

A CFD program can be used to calculate airflow distribution around buildings. This flow distribution provides valuable information for the design of natural ventilation and a comfortable outdoor environment. Fig. 3(a) shows the preliminary site design (Scheme I) of an apartment building complex in Beijing. The design uses 16 high-rise buildings ranging from 33 to 90 m high. The building site has a prevailing wind from the north in the winter. With this design, the wind speed at a height of 1.5 m above the ground in section 1-1 is around 8 ~ 9m/s (Grade 5) as shown in Fig. 4(a). This is too high to be acceptable even for a short stay in the winter. The reason is that the wind can pass freely through the linear arrangement of the buildings. Furthermore, the CFD calculation shows that at a height of 30 m, the wind speed among most of the buildings is 9~10 m/s, and at a height of 70 m, the wind speed is above 12 m/s (Grade 6). The high wind speed leads to excessively high infiltration in the winter and difficulties in using the wind for natural ventilation in the summer. Therefore, the building site should be redesigned, and the height of the buildings should be reduced.

Based on the airflow distribution for Scheme I, Scheme II was developed, as shown in Fig. 3(b). Scheme II used a lower building height ranging from 20 to 60 m to reduce winter infiltration without compromising the population density. The improved design protects the buildings from the north wind in the winter by using relatively high buildings in the north.

Fig. 4(b) shows that the discomfort problem is greatly reduced in Scheme II, but there are still some problems. For example, in entrances A, B, and C, the wind speed is very high because of the linear arrangement. Staggering the entrances can easily solve this problem. Moreover, natural ventilation in summer may not be effective in Scheme II. As shown in Fig. 3(b), more than half of the buildings have long sides facing east and west, such as Buildings 1-8. Since the prevailing wind in the summer is from the south in this site, the buildings with the long sides facing east and west may not be able to take advantage of natural ventilation, such as cross ventilation. In addition, the orientation is not good for passive heating design and it is difficult to shade the buildings from strong solar radiation in the summer.

Therefore, Scheme III was finally developed as shown in Fig. 3(c). The low-rise buildings are now tilted 45^{o}, thus having the long side facing south-east and north-west. In Scheme III, both the outdoor thermal comfort and natural ventilation are considered. Fig. 4(c) shows that the high-rise buildings on the north side can block the high wind from the north in winter. As a result, the wind speed at the site is small. Although, at entrances A and B, the wind speeds are relatively high (about 7~10 m/s), the impact on the pedestrians' comfort is small, since these entrances for cars.

In the summer, the south wind prevails on the site. Fig. 4(d) shows that the wind speed around most of the buildings at 1.5 m above the ground is above 1.0 m/s. This wind speed is sufficiently high for natural ventilation. The tilted building arrangement helps to introduce more wind into the site. Furthermore, the staggered arrangement prevents the front buildings from blocking the winds. Therefore, Scheme III provides good outdoor thermal comfort and potential to use natural ventilation.

Evaluation of natural ventilation performance

A CFD program has also been used to evaluate the performance of natural ventilation design in a building. The most important evaluation criterion is the air temperature in the building. By using the concept of coupling a CFD program with an energy simulation program, the air temperature can be determined.

In this study, a generic apartment building in Beijing with heavy concrete floor and ceiling slabs was investigated. According to the climate data analysis, night cooling seems to be a good natural ventilation strategy. The building envelope is opened to allow natural ventilation during the night hours when outdoor air temperature is lower than the indoor air temperature; the building structure is then cooled down. During the daytime, when the outdoor temperature becomes higher than the indoor air temperature, the building envelope is closed. The cooled structure then absorbs the internal heat to maintain a comfortable indoor environment. A CFD program was used to calculate the air exchange rate in the building with night cooling while an energy simulation program was used to determine the air temperature.

Fig. 5 shows the calculated indoor air temperature and the corresponding outdoor air temperature in the warm season. The air temperature in the living room is 3.9 K lower than the outside air temperature, although there are internal heat gains.

VOC emission studies

The CFD technique can study not only the distribution of flow, temperature, and chemical species in room air, but also the heat and mass transfer in solid materials. This is especially useful for indoor air quality studies. For example, numerous field and laboratory studies have found that commonly used building materials, such as wood products, floor coverings (carpet, vinyl), wall coverings (wallpaper, fabric), ceiling materials (acoustic tiles, subfloors), and insulation materials (fiberglass, rigid foam) emit a variety of volatile organic compounds (VOCs). Emissions from the building materials are important to indoor air quality because of their large surface area and permanent exposure to indoor air.

Consider a material source that has one surface exposed to the air. VOC emissions from this source include the mass transfer in three different regions:

- The solid material
- The material-air interface
- The bulk air

For a dry material with homogeneous diffusivity, the following diffusion model has been used to describe the VOC mass transport within the material:

$$\frac{\partial C_m}{\partial t} = \frac{\partial}{\partial x_j}\left(D_m \frac{\partial C_m}{\partial x_j}\right) \tag{13}$$

At the material-air interface, a VOC phase change occurs from the material side to the air side. For low concentrations, the equilibrium condition at the material-air interface may be described by:

$$C_m = K_{ma} C_a \tag{14}$$

Then Eq. (1) is used to calculate the air velocity distribution and the VOC mass transfer from the material-air interface to the ambient air.

Recently, different specimens of particleboard have been studied with the above mentioned model for their VOC emissions. This approach uses the following parameters to describe emission characteristics: the initial VOC concentrations in the material (C_0), the solid-phase diffusion coefficient (D_m), the material-air partition coefficient (K_{ma}), and the age of the material (AGE). These parameters were obtained by fitting the predicted VOC concentrations with the small-scale chamber data.

Fig. 6 compares the predicted major VOC concentrations and the data measured from a small test chamber. The results show that pre-determining the K_{ma} and AGE and adjusting the D_m and C_0 can achieve a fairly good agreement of VOC concentrations between the experimental data and model prediction. The investigation has found that different parameters have different impacts on emissions. The emission rate is proportional to C_0. D_m influences both short-term and long-term emissions. A higher D_m results in a higher initial emission rate and a faster decay rate. On the other hand, K_{ma} and AGE affect only the short-term emissions of the particleboard, having virtually no impact on long-term emissions.

LES Studies

The above examples show that the RANS models are useful for indoor and outdoor environment design. However, these models have too many coefficients to be tuned in order to obtain a correct solution. Even for an experienced CFD user, it is difficult to select a suitable turbulence model and its coefficients. On the other hand, LES has only one or no empirical coefficient; thus it sounds superior to the RANS models. Therefore, LES has been used for the study of indoor and outdoor environment.

LES requires the separation of small-eddies from large-eddies with a filter. For simplicity, the following section uses a one-dimensional notation. The filtered velocity is

$$\overline{u_i} = \int G(x, x')u_i(x)dx' \tag{15}$$

where G(x, x') is a filter function. The filter function is large only when G (x, x') is less than the filter width, a length scale over which the averaging is performed. The flow eddies larger than the filter width are "large-eddies," and those smaller than the width are "small-eddies".

This paper uses a box filter, i.e.

$$G(x_i) = \begin{cases} \dfrac{1}{\Delta_i} & (|x_i| \le \dfrac{\Delta_i}{2}) \\ 0 & (|x_i| > \dfrac{\Delta_i}{2}) \end{cases}, \tag{16}$$

With the finite volume method, it seems natural to define the filter width, $\Delta_i = (\Delta x_1 \Delta x_2 \Delta x_3)^{\frac{1}{3}}$, as an average over a grid volume.

With the filter, it is possible to derive the governing conservation equations for momentum (Navier-Stokes equations), mass continuity, and energy. The filtered Navier-Stokes equations for an incompressible flow are:

$$\frac{\partial \overline{u_i}}{\partial t} + \frac{\partial}{\partial x_j}(\overline{u_i} \cdot \overline{u_j}) = -\frac{1}{\rho}\frac{\partial \overline{P}}{\partial x_i} + \upsilon \frac{\partial^2 \overline{u_i}}{\partial x_i \partial x_j} - \frac{\partial \tau_{ij}}{\partial x_j} + g_i \beta(\overline{T} - \overline{T}_0) \tag{17}$$

where the subgrid Reynolds stresses are

$$\tau_{ij} = \overline{u_i u_j} - \overline{u_i} \cdot \overline{u_j} \tag{18}$$

$\overline{u_i u_j}$ is unknown and needs to be modeled.

In order to close the equations, the subgrid Reynolds stresses can be modeled using the Smagorinsky model (1963).

$$\tau_{ij} = 2C\ \overline{\Delta}^2 \left|\overline{S}\right| \overline{S}_{ij} \tag{19}$$

where $\left|\overline{S}\right| = (2\overline{S_{ij}} \cdot \overline{S_{ij}})^{\frac{1}{2}}$, $\overline{S_{ij}} = \frac{1}{2}(\frac{\partial \overline{u_i}}{\partial x_j} + \frac{\partial \overline{u_j}}{\partial x_i})$ $C = C_s^2, C_s = 0.1 \sim 0.25.$

However, the Smagorinsky model coefficient C is an empirical coefficient that depends on flow.

Ideally, C should be determined as a function of flow through a Dynamic Subgrid-scale Model (DSM) (Germano et al. 1991). DSM calculates the model coefficient by relating the subgrid scale Reynolds stresses to two different filter sizes. Since the Reynolds stresses vary with time and location, the resulting model coefficient is therefore also a function of time and location.

DSM uses an explicit test filter, $\widetilde{G}$, with a filter width of $\widetilde{\Delta}$ $(\widetilde{\Delta} = 2\overline{\Delta})$ (Germano et al. 1991) to determine the turbulent stresses on the test filter ($\widetilde{G}$ filter).

$$T_{ij} = \widetilde{\overline{u_i u_j}} - \widetilde{\overline{u}}_i \widetilde{\overline{u}}_j \tag{20}$$

The first term on the right side of Eq. (20) cannot be determined directly, like the one in Eq. (18). However, substituting Eq. (20) and Eq. (18) with a test filter can eliminate the terms

$$T_{ij} - \widetilde{\tau}_{ij} = L_{ij} \tag{21}$$

where $L_{ij} = \widetilde{\overline{u}_i \overline{u}_j} - \widetilde{\overline{u}}_i \widetilde{\overline{u}}_j$

The resolved turbulent stresses, L_{ij}, in Eq. (21) can be calculated explicitly. With the definition of the Smagorinsky model, the DSM coefficient C can be determined. However, the DSM requires averaging the coefficient over a homogeneous flow direction (statistical homogeneity) since the coefficient fluctuates significantly. The averaging procedure can dampen large fluctuations of C often encountered in a flow prediction. This procedure gives good results

for simple flows with at least one homogeneous direction, such as a turbulent channel flow. However, it cannot be used for a flow without a homogeneous direction, such as room airflow.

Another approach by Meneveau et al. (1996) used a Lagrangian dynamic model. This model is suitable for inhomogeneous flows and the results look encouraging. The model needs an additional parameter, the Lagrangian averaging time, which must be prescribed. Additional tests are required to establish how to calculate this parameter (Moin 1998).

Therefore, a DSM model is being developed that calculates an indoor airflow without a homogeneous flow direction.

Filtered dynamic sub-grid scale model (FDSM)

Note that all of the terms in Eq. (21) are related to the test filter ($\widetilde{\Delta}$). The model coefficient C obtained with Eq. (21) should be valid for the test filter ($\widetilde{\Delta}$). Since the subgrid scale Reynolds stresses, τ_{ij}, are defined with the grid filter ($\overline{\Delta}$), the model coefficient C should be related to the grid filter ($\overline{\Delta}$). This can be done by applying a grid filter to Eq. (21) to yield

$$\overline{T}_{ij} - \overline{\widetilde{\tau}}_{ij} = \overline{L}_{ij} \tag{22}$$

In order to obtain a new model coefficient from Eq. (22), the τ_{ij} and the T_{ij} in Eq. (22) are modeled by using the Smagorinsky model or the mixed model (Zang 1993). However, this modeling leads to an error in satisfying Eq. (22):

$$e_{ij} = \overline{L}_{ij} - \overline{C_T\,\alpha_{ij}} + \overline{\widetilde{C_\tau\,\beta_{ij}}} = \overline{L}_{ij} - C\overline{M}_{ij} \tag{23}$$

where $\alpha_{ij} = 2\overline{\widetilde{\Delta}}^2 \left|\overline{\widetilde{S}}\right| \overline{\widetilde{S}}_{ij}$, $\beta_{ij} = 2\overline{\Delta}^2 \left|\overline{S}\right| \overline{S}_{ij}$, and $M_{ij} = \alpha_{ij} - \widetilde{\beta}_{ij}$.

We have used the least-square approach to obtain the model coefficient, C in Eq. (23), as suggested by Lilly (1992) and Ghosal et al. (1995). At any given point in a space, **x**, the e_{ij} is a function of the C. In order to obtain an optimal C, the e_{ij} should be integrated over the entire flow domain with a smooth function, because the square of the residual, $e_{ij}e_{ij}$, may have locally violent changes. The integrated square of the error function, $E_{ij}(C)$, is

$$E_{ij}(C) = \int G_f(\mathbf{x},\mathbf{x}')\, e_{ij}(\mathbf{x}')\, e_{ij}(\mathbf{x}')\, d\mathbf{x}' \tag{24}$$

where $G_f(\mathbf{x},\mathbf{x}')$ is a smooth function. By substituting Eq. (23) into Eq.(24), Eq. (24) reads:

$$E_{ij}(C) = \int G_f(\mathbf{x},\mathbf{x}')(\overline{L}_{ij} - C\overline{M}_{ij})^2\, d\mathbf{x}' \tag{25}$$

Since the least square condition for Eq. (24) is $\dfrac{\partial E_{ij}(C)}{\partial C} = 0$, the optimal model coefficient C is obtained as:

$$C = \frac{\int G_f(\mathbf{x},\mathbf{x}')\,\overline{L}_{ij}\overline{M}_{ij}\,d\mathbf{x}'}{\int G_f(\mathbf{x},\mathbf{x}')\,\overline{M}_{ij}\overline{M}_{ij}\,d\mathbf{x}'} \tag{26}$$

The C is clearly a function of time and space, and it can be applied to inhomogeneous flows. The smooth function, $G_f(\mathbf{x},\mathbf{x}')$, should be chosen for the entire flow domain and may depend on the turbulent scales. Although the smooth function can be in many forms, a box filter (Eq. (16)) may be the most convenient ($G_f(\mathbf{x},\mathbf{x}') = G(\mathbf{x},\mathbf{x}')$). The filter can be either a grid filter or a test filter

$$C = \frac{\overline{\overline{L}_{ij}\overline{M}_{ij}}}{\overline{\overline{M}_{ij}\overline{M}_{ij}}} \quad \text{(with the grid filter } \overline{\Delta}\text{)} \tag{27}$$

or

$$C = \frac{\overline{L}_{ij}\overline{M}_{ij}}{\widetilde{\overline{M}_{ij}\overline{M}_{ij}}} \quad \text{(with the test filter } \widetilde{\overline{\Delta}}\text{)} \tag{28}$$

Eqs. (27) and (28) are now defined as the filtered dynamic subgrid scale model (FDSM). The $FDSM_G$ has the grid filter in Eq. (27), and the $FDSM_T$ has the test filter in Eq. (28). The function of the grid filter is to average the coefficient and to smooth the large fluctuation of the coefficient. The filter technique will lead to a stable numerical solution. The FDSM can be considered as a simple model compared with those proposed by Ghosal et al. (1995) and Meneveau et al. (1996). The model can be used for flow without a homogenous direction.

The $FDSM_G$ or $FDSM_T$ can also be locally negative. According to Piomelli et al. (1991), a negative C indicates a negative eddy viscosity and implies an energy transfer from small scales to the resolved scales or backscatter. However, the negative C can also lead to a numerical instability. In order to avoid the instability, the present investigation uses C = Max (0.0, Eq.(27) or (28)).

We have applied the FDSM for mixed convection flow in a room, as shown in Fig. 7(a). Blay et al. (1992) measured the air velocity, temperature, and turbulent energy distributions for this case. The geometry of the test rig was H = 1.04 m, L = 1.04 m, and D = 0.7 m. This test rig is a scale-model of a room and has a homogeneous direction (the depth direction) so that the DSM can also be used. The inlet height, h_{in}, was 0.018 m, the supply air velocity, U_{in}, was 0.57 m/s, and the supply air temperature, T_{in}, was 15°C. The outlet height was 0.024 m. The test rig used a floor heating system with a floor temperature, T_f, of 35°C. All other wall temperatures were 15°C. The corresponding Archimedes number ($Ar = \frac{\beta g h_{in}(T_f - T_{in})}{U_{in}^2}$) was 0.0036, and the Reynolds number ($Re = \frac{U_{in} h_{in}}{\nu}$) was 678.

The computations used a non-slip velocity condition for all the walls. The meshes employed were $62 \times 62 \times 12$ for the height (x), width (y), and depth (z) directions.

Figs. 7(b) and 7(c) show the measured mean air velocity distribution and the averaged air velocity distribution using the $FDSM_G$. The measured and computed airflow patterns are almost

the same. The LES simulation shows a small re-circulation in the left-bottom corner, but not in the experiment. It is not clear whether this is due to insufficient fine measuring points or due to the numerical model used.

Fig. 8 further compares the predicted mean air velocity, temperature, and turbulent energy distributions using the DSM, $FDSM_{G,}$ and $FDSM_T$ with the experimental data at two center sections (at x = 0.502 m and y = 0.502 m). Fig. 8(a) shows that the three subgrid scale models give very similar air velocity profiles. The $FDSM_G$ performed slightly better than the others. The predicted velocity profiles agree reasonably well with the experimental data.

However, Figs. 8(b) indicates that the predicted air temperature using the three models is about 1.5 K higher than the measured one, though the shape of the predicted temperature profiles is the same as the measured one. The models may overpredict the heat transfer from the floor or underpredict the heat transfer to the other walls. Since no detailed measurements on the heat transfer were available, it is difficult to identify the actual cause of these discrepancies. Perhaps the subgrid scale Prandtl number was not correctly modeled for the buoyancy effect.

Fig. 8(c) illustrates the computed turbulent energy ($k^{1/2} = \{(u'^2+v'^2+w'^2)/2\}^{1/2}$) profiles at section x = 0.502 m and the comparison with the corresponding experimental data. The performance of the $FDSM_G$ and DSM in predicting the turbulence energy distribution was good, while the performance of the $FDSM_T$ was poor.

LES applications

We have used LES to further study complicated indoor and outdoor environment problems. For example, Fig.1 shows that an LES program can successfully calculate the air velocity and temperature in an office with displacement ventilation. The LES simulation provides more information than the RANS modeling, such as power spectrum of turbulence. The power spectrum of turbulence can be a very important comfort parameter. Our application of LES for outdoor airflow simulation can be found in another paper (Spengler and Chen 2000). Unfortunately, the computing time needed for LES is much higher than that for RANS modeling. At present, LES can only be performed in powerful workstations and super computers. Only simple LES can be done on a high end PC.

Concluding Remarks

This paper summarizes some recent studies on indoor and outdoor environment problems conducted at the Massachusetts Institute of Technology by using CFD tools. Our effort focuses not only on the development of RANS and LES models for indoor and outdoor environment studies but also on their applications for complicated and practical problems. The CFD tools are powerful for solving the problems, although they need skillful users, as well as large and fast computers.

The two-layer turbulence model enables us to predict accurate heat transfer on a wall. The computing time needed is slightly higher than that by the standard k-ε model but much lower than that by a low-Reynolds number k-ε model.

The zero-equation turbulence model can significantly reduce computing costs. For a simple room, the computing time needed is just a few minutes for a steady-state solution on a PC. The coupling of a CFD program with the zero-equation model with an energy simulation

program can be used more accurately and informatively for building energy analysis and indoor environment design.

The CFD program is a powerful tool to predict airflow in and around buildings to design a thermally comfortable indoor or outdoor environment. Architects and engineers can work together to design buildings that shield winter wind and allow summer natural ventilation. The software developed can further evaluate the performance of natural ventilation in a building.

The CFD tool can be extended to include VOC diffusion in building materials and mass transfer at solid-air interfaces. This tool can then be used to predict VOC emissions from the building materials and indoor air quality in the room.

A new dynamic subgrid-scale model has been developed to predict indoor airflow without a homogenous flow direction. The model uses two different filters to obtain the model coefficient as a function of space and time. The model can accurately predict flow in a room with a heated floor and in an office with displacement ventilation. Although the computing costs with LES are high at present, the computed results are very informative.

Acknowledgement

The authors would like to thank the contributions from their colleagues at MIT (in alphabetical order): Mr. G. Carrilho-da-Graça, Prof. L.R. Glicksman, Ms. Y. Jiang, Prof. L.K. Norford, Prof. A.M. Scott, Dr. M. Su, Dr. W. Xu, Dr. X. Yang, Dr. X. Yuan, and Dr. W. Zhang. This work is supported by the U.S. National Science Foundation under grants CMS-9623864 and CMS-9877118, by ASHRAE through contracts RP-927 and RP-949, and by the V. Kahn-Rasmussen Foundation, the Center for Indoor Air Research, and the Archilife Research Foundation.

References

Blay, D., Mergui, S. and Niculae, C. 1992. "Confined turbulent mixed convection in the presence of a horizontal buoyant wall jet," *Fundamentals of Mixed Convection*, *ASME HTD-Vol. 213,* pp. 65-72.

Chen, Q. 1995. "Comparison of different k-ε models for indoor airflow computations," *Numerical Heat Transfer, Part B: Fundamentals*, 28, 353-369.

Chen, Q. 1996. "Prediction of room air motion by Reynolds-stress models," *Building and Environment*, 31(3), 233-244.

Chen, Q., 1997, "Computational fluid dynamics for HVAC: successes and failures," *ASHRAE Transactions*, 103 (1), 178-187.

Davidson, L. and Nielsen, P.V. 1996. "Large eddy simulations of the flow in a three-dimensional ventilated room," *Proc. of Roomvent '96*, Vol. 2, pp. 161-168, Yokohama, Japan.

Davidson, L. and Nielsen, P.V. 1998. "A study of low-Reynolds number effects in back-facing step flow using large eddy simulation," *Proc. of Roomvent '98*, Vol. 1, pp. 125-132, Stockholm, Sweden.

Deardorff, J.W. 1970. "A three-dimensional numerical study of turbulent channel flow at large Reynolds numbers," *J.Fluid Mechanics*, 41, 453.

Emmerich, S. and McGrattan, K. 1998. "Application of a large eddy simulation model to study room airflow," *ASHRAE Transactions*, 104(1).

Germano, M., Piomelli, U., Moin, P. and Cabot, W.H. 1991. "A dynamic subgrid-scale eddy viscosity model," *J. Physics Fluids* A, 3, 1760.

Ghosal, S., Lund, T., Moin, P. and Akselvoll, K. 1995. "A dynamic localization model for large-eddy simulation of turbulent flows," *J. Fluid Mechanics,* 286, 229.

Kasagi, N. and Nishimura M. 1997. "Direct numerical simulation of combined forced and natural convection in a vertical plane channel," *Int. J. Heat and Fluid Flow*, 18, 88-99.

Launder, B.E. and Spalding, D.B. 1974. "The numerical computation of turbulent flows," *Computer Method in Applied Mechanics and Energy*, 3, 269-289.

Lilly, D.K. 1992. "A proposed modification of the Germano subgrid-scale closure method," *J. Physics Fluids* A, 4, 633.

Meneveau, C., Lund, T. and Cabot, W. 1996. "A Lagrangian dynamic sub-grid scale model of turbulence," *J. Fluid Mechanics*, 315, 353.

Moin, P. 1998. "Numerical and physiscal issues in large eddy simulation of turbulent flows," *JSME Int. J.* B, 41(2), 454.

Murakami, S. 1993. "Comparison of various turbulence models applied to a bluff body," *J. Wind Engineering and Industrial Aerodynamics*, 46-47, 21-36.

Murakami, S., 1998, "Overview of turbulence models applied in CWE-1997," *J. Wind Engineering and Industrial Aerodynamics*, 74-76, 1-24.

Piomelli, U., Cabot, W.H., Moin, P. and Lee, S. 1991. "Subgrid-scale backscatter in turbulent & transitional flows," *J. Physics Fluids* A, 3, 1766.

Smagorinsky, J. 1963. "General circulation experiments with the primitive equations, I: The basic experiment," *Monthly Weather Rev.,* 91, 99-164.

Spengler, J.D. and Chen, Q. 2000. "Designing a healthy building," Submitted to *Annual Review of Energy and the Environment.*

Xu, W. 1998. "New turbulence models for indoor airflow simulation," *Ph.D. Thesis*, Department of Architecture, Massachusetts Institute of Technology, Cambridge, MA

Yang, X., 1999. "Study of building material emissions and indoor air quality," *Ph.D. Thesis*, Department of Architecture, Massachusetts Institute of Technology, Cambridge, MA.

Yuan, X., Chen, Q., Glicksman, L.R., Hu, Y., and X. Yang. 1999. "Measurements and computations of room airflow with displacement ventilation," *ASHRAE Transactions*, 105(1), 340-352.

Zang, Y., Street, R.L. and Koseff, J.R. 1993. "A dynamic mixed subgrid-scale model and its application to recalculating flow," *J. Physics Fluids* A, 5, 3186.

Zhang, W. and Chen, Q. 2000. "Large eddy simulation of indoor airflow with a filtered dynamic subgrid scale model," Accepted by *Int. J. Heat Mass Transfer*.

Table 1. Values of Φ, Γ_ϕ and S_ϕ in Eq. (1).

Equation	Φ	$\Gamma_{\Phi,eff}$	S_Φ
Continuity	1	0	0
Momentum	U_i (i=1,2,3)	$\mu+\mu_t$	$-\partial P/\partial x_i - \rho g_i\beta(T-T_0)$
T-equation	T	$\mu/\sigma_l + \mu_t/\sigma_t$	S_T
k-equation	k	$(\mu+\mu_t)/\sigma_k$	$G-\rho\varepsilon+G_B$
ε-equation	ε	$(\mu+\mu_t)/\sigma_\varepsilon$	$[\varepsilon(C_{\varepsilon1}G-C_{\varepsilon2}\rho\varepsilon)/k]+C_{\varepsilon3}G_B(\varepsilon/k)$
Species	C	$(\mu+\mu_t)/\sigma_c$	S_C
$\mu_t=\rho C_\mu k^2/\varepsilon$ $G=\mu_t(\partial U_i/\partial x_j+\partial U_j/\partial x_i)\partial U_i/\partial x_j$ $G_B=-g(\beta/C_P)(\mu_t/\sigma_{T,t})\partial T/\partial x_i$			
$C_{\varepsilon1}=1.44$, $C_{\varepsilon2}=1.92$, $C_{\varepsilon3}=1.44$, $C_\mu=0.09$ $\sigma_t=0.7$, $\sigma_t=0.9$, $\sigma_k=1.0$, $\sigma_\varepsilon=1.3$, $\sigma_C=1.0$			

Table 2. The grid number and computing time used with the zero-equation model.

Case	Grid number	Computing time [min:sec]
Infiltration	27×22×20	6:46
Partition	26×20×15	6:11
Displacement ventilation	25×18×16	4:41

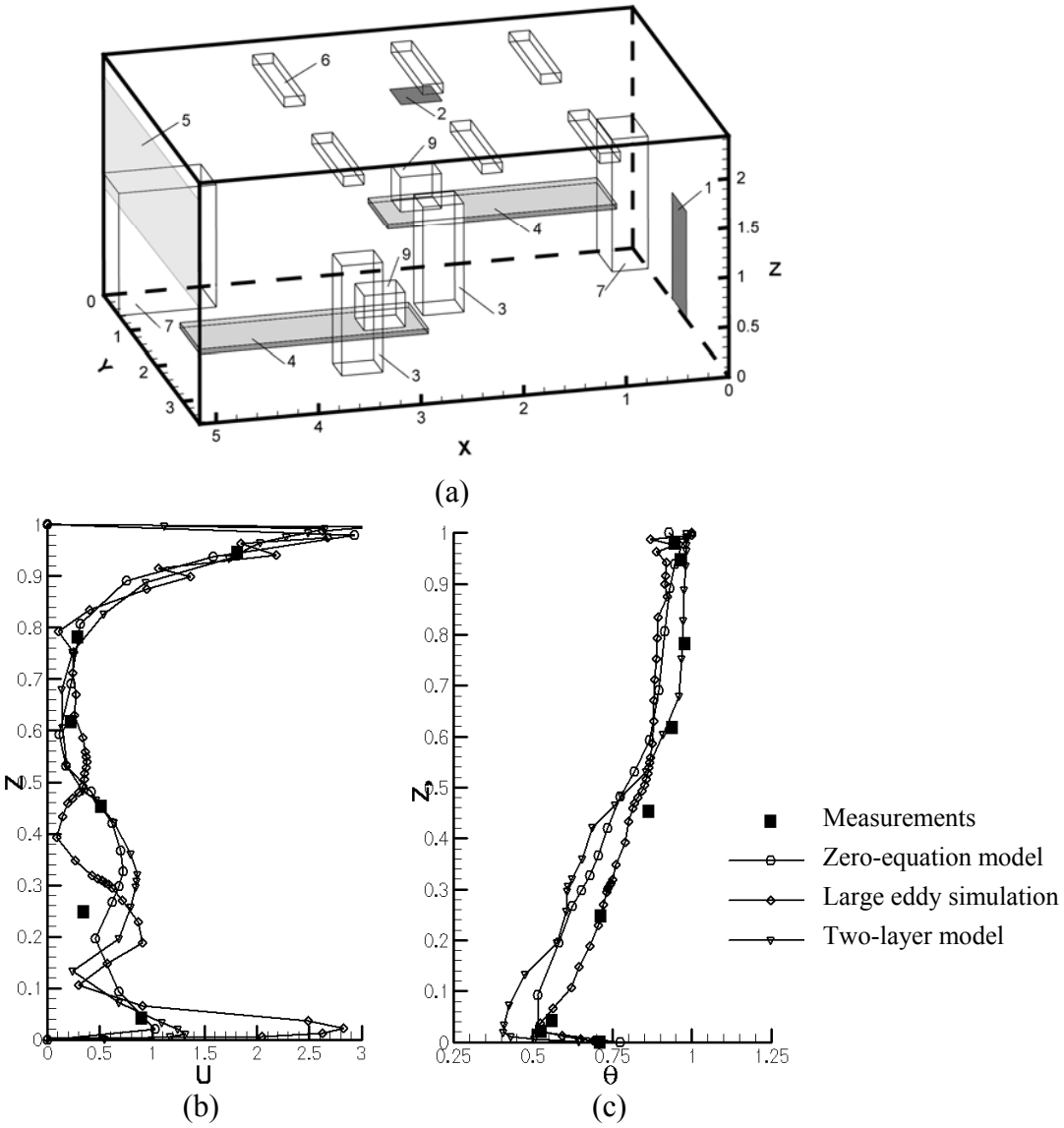

Fig. 1. Velocity and temperature distribution at the center of an office with displacement ventilation, (a) the office layout of the office (1-inlet, 2-outlet, 3-person, 4-table, 5-window, 6-fluorescent lamps, 7-cabinet, 8-baseboard heater, 9-computer, 10-partition wall), (b) velocity profile, (c) temperature profile.

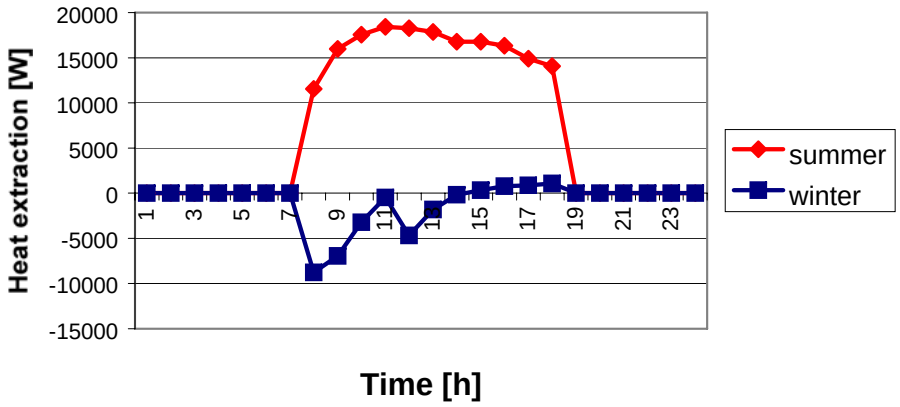

(a) Heat extraction

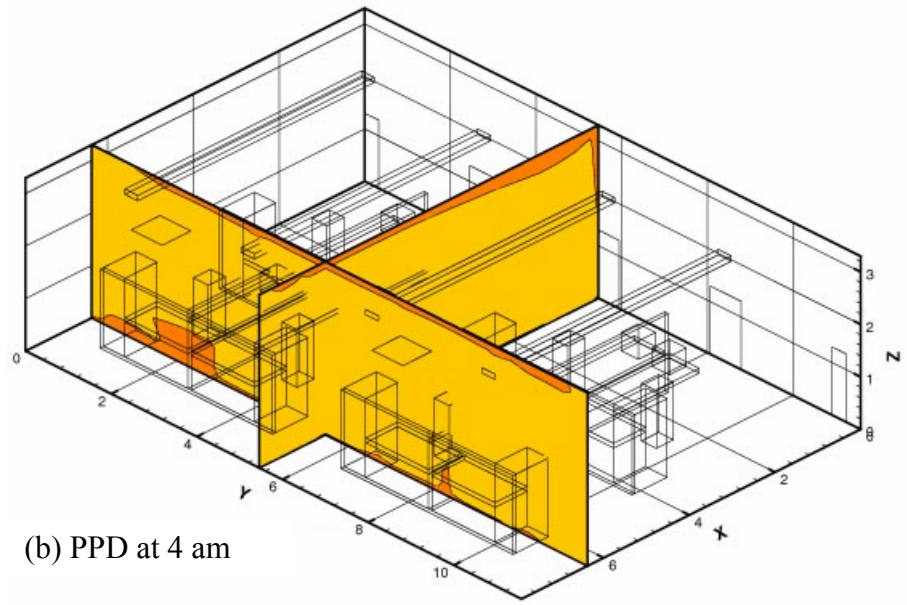

(b) PPD at 4 am

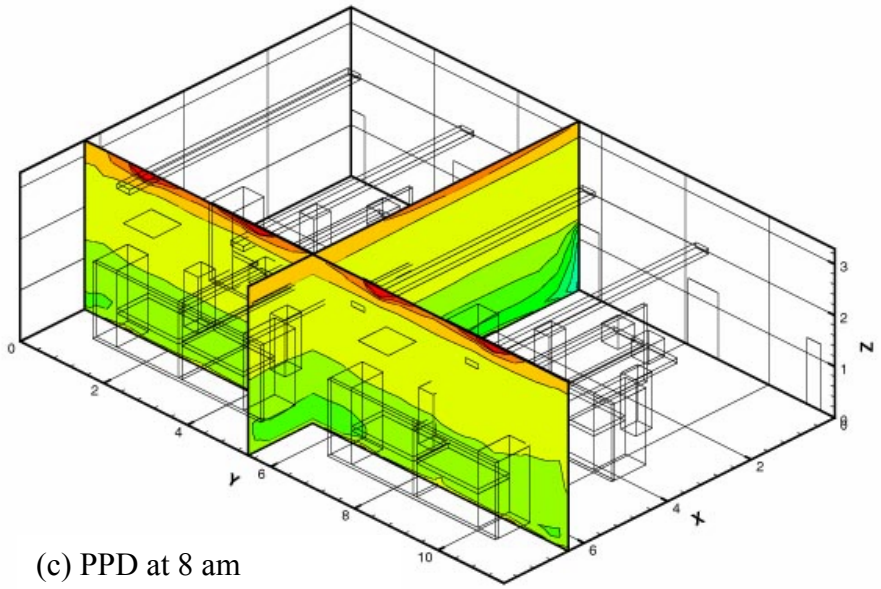

(c) PPD at 8 am

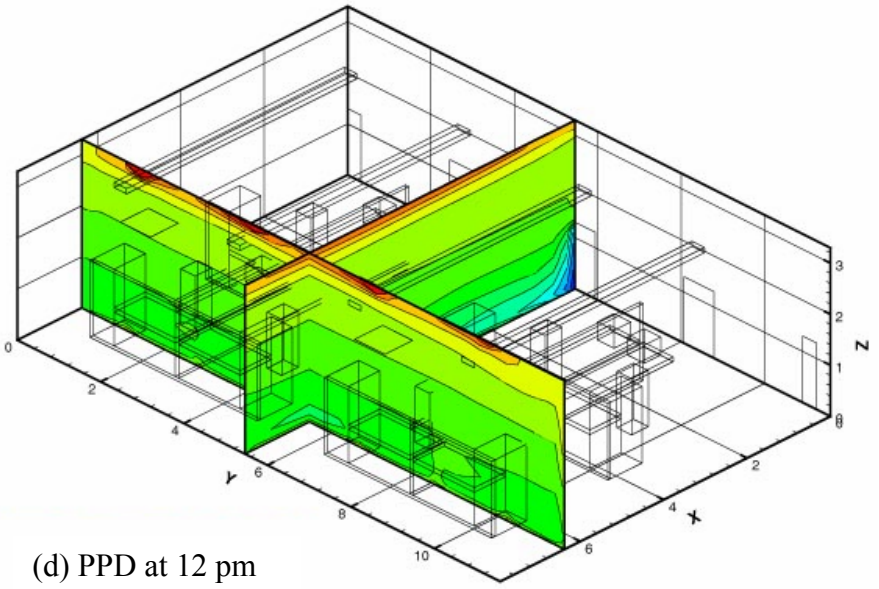

(d) PPD at 12 pm

Fig. 2 The simulated results for a large office by the coupled CFD and energy analysis program.

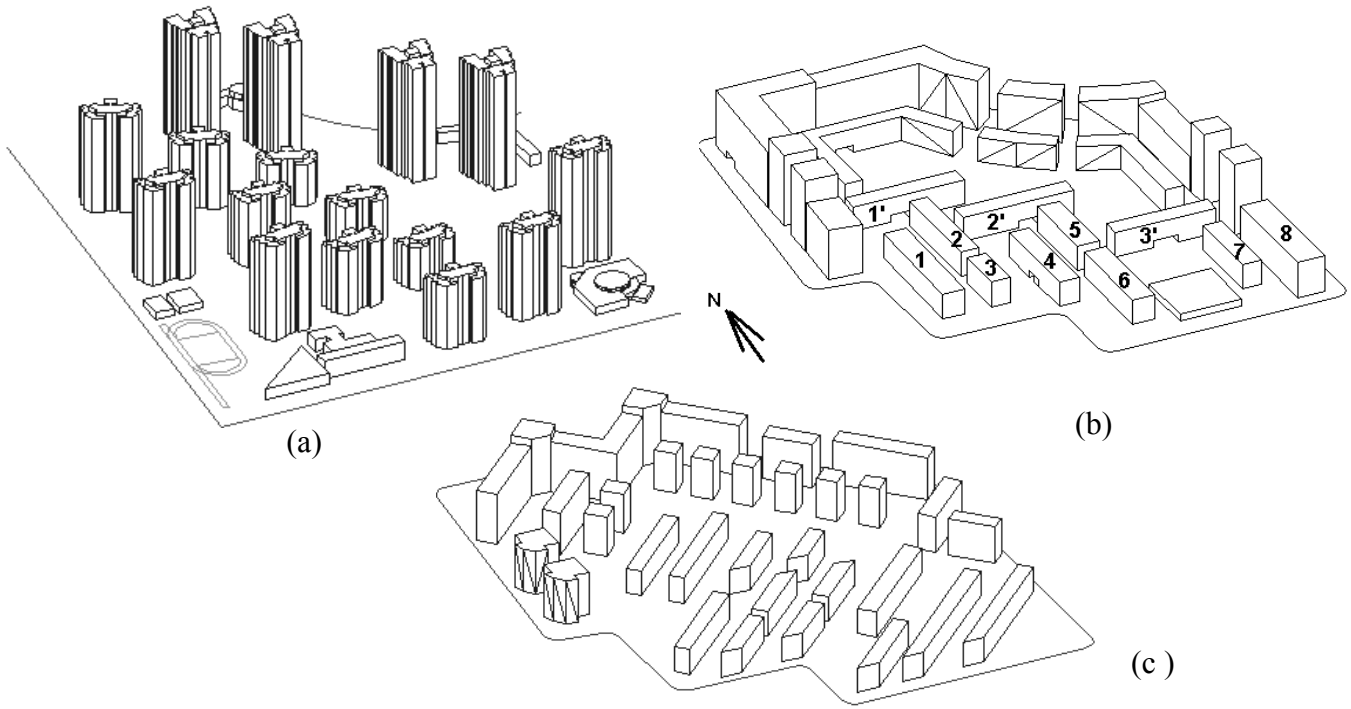

Fig. 3 Three designs for the apartment building complex: (a) Original design (Scheme I), (b) first improved design (Scheme II), and (c) final design (Scheme III).

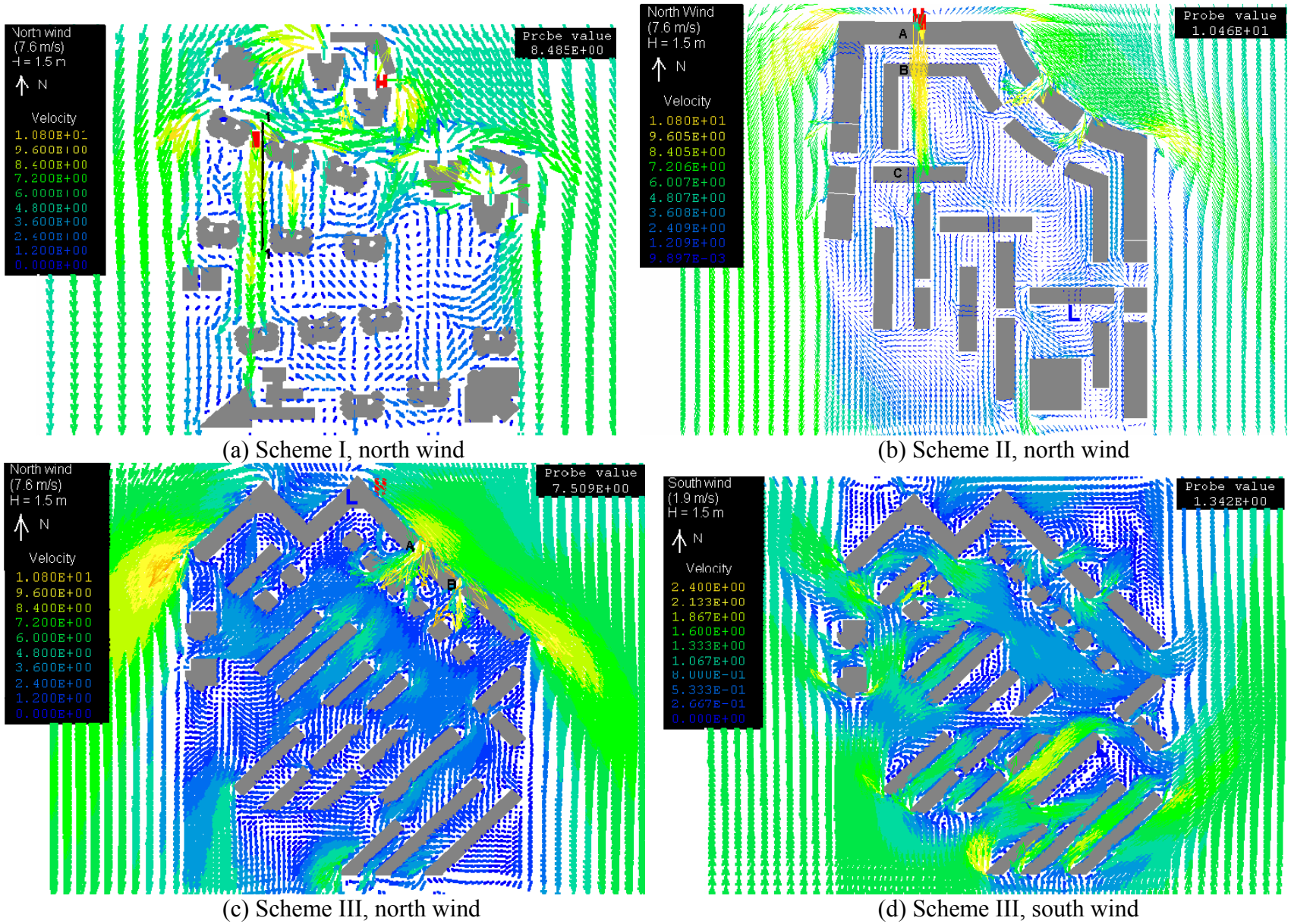

(a) Scheme I, north wind

(b) Scheme II, north wind

(c) Scheme III, north wind

(d) Scheme III, south wind

Fig. 4 Wind velocity distribution at the height of 1.5 m above the ground around the buildings.

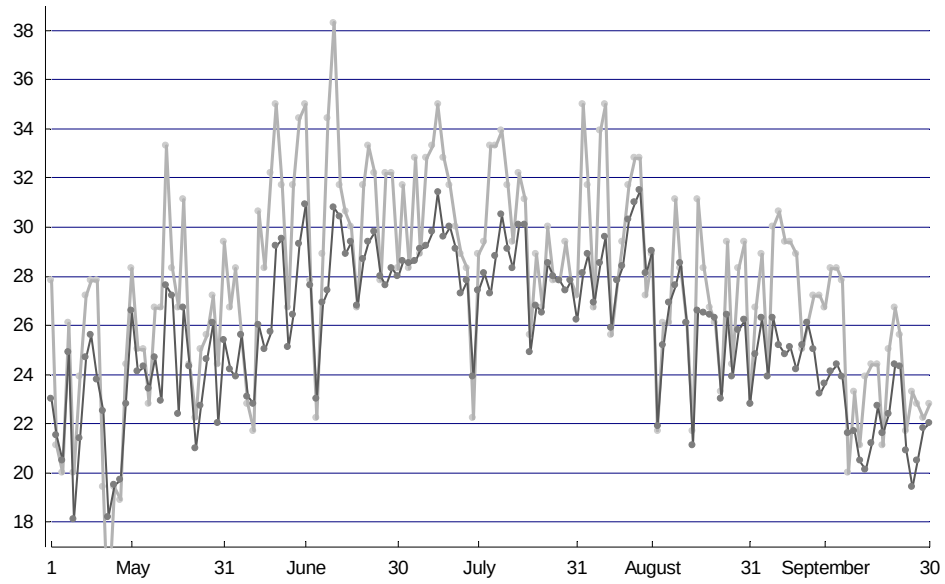

Fig. 5 Daily maximum air temperature in the living room with night cooling (dark gray) and outside (light gray) in Beijing.

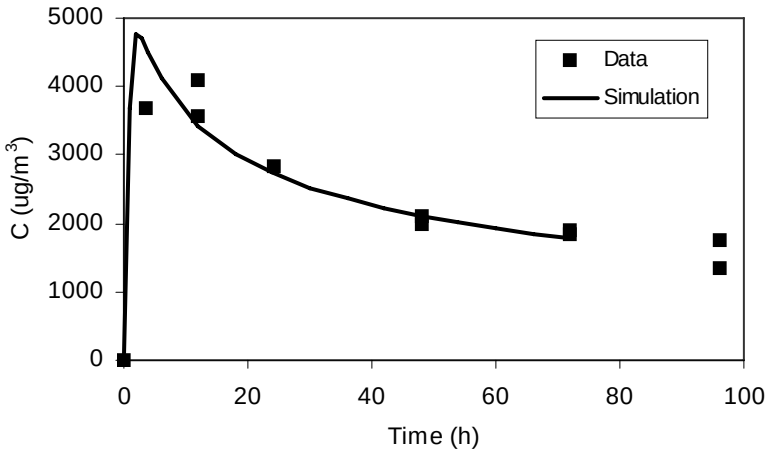

(a)

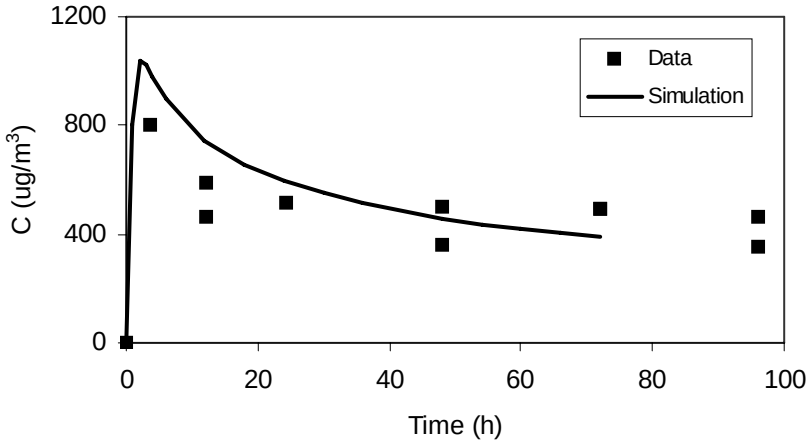

(b)

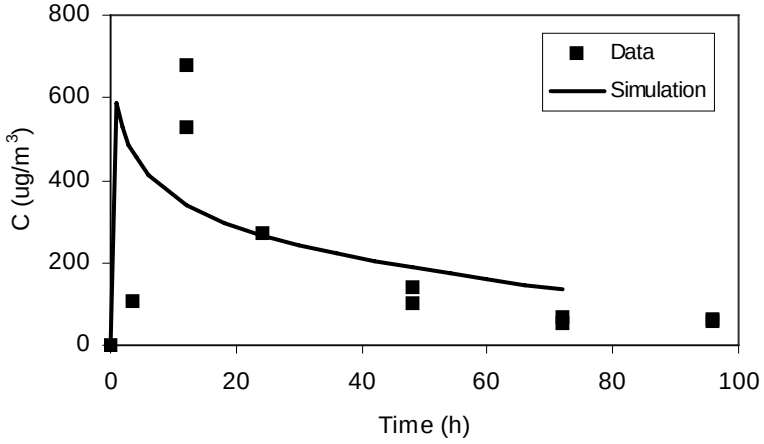

(c)

Fig. 6 Comparison of measured and simulated VOC concentrations emitted from the particle board: (a) TVOC, (b) Hexanal, (c) α.pinene

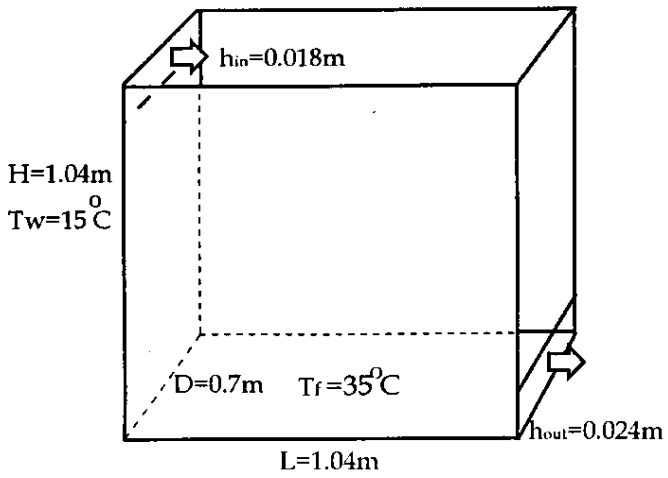

(a)

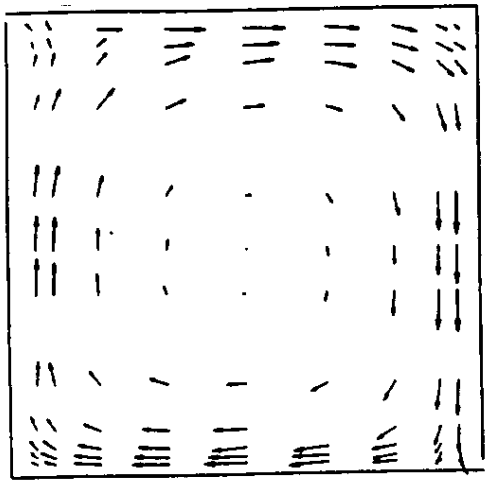

(b)

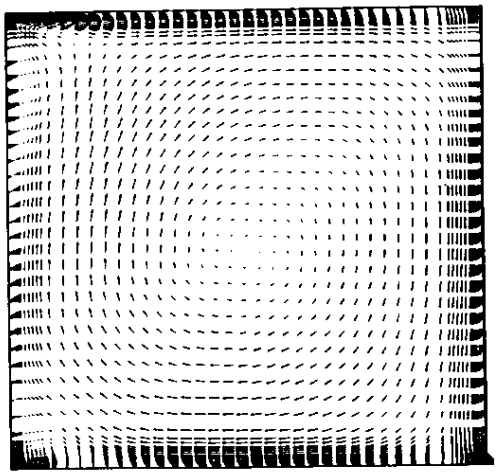

(c)

Fig. 7 The predicted and measured mixed convection flow in a room. (a) room geometry, (b) average velocity vectors obtained from the experiment (Baly et al,1992), (c) average velocity vectors computed by the $FDSM_G$

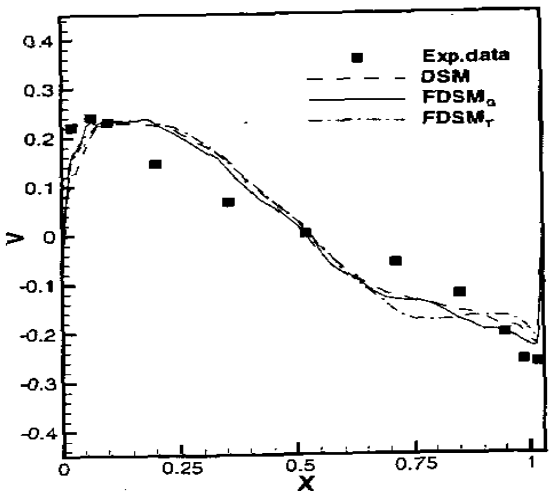

(a)

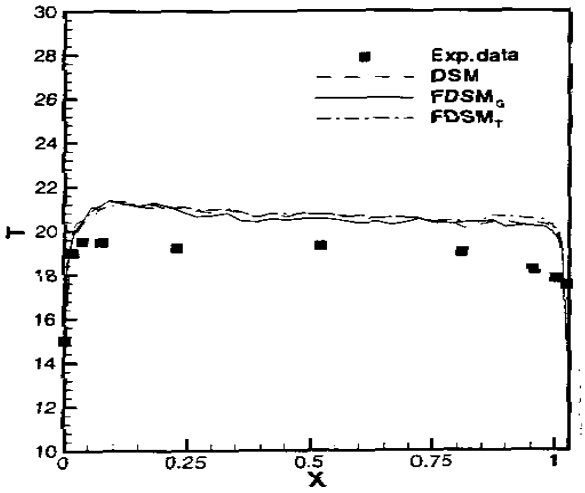

(b)

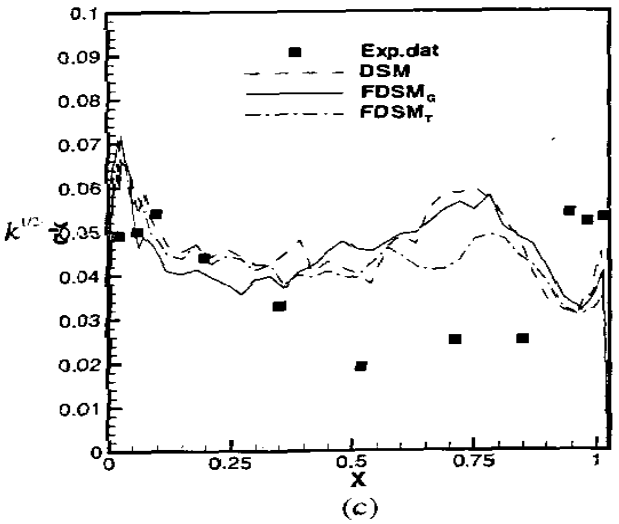

(c)

Fig. 8 Comparison of the predicted and measured results on the center sections (X=0.502m). (a) average velocity, (b) average temperature, (c) average turbulent energy ($k^{1/2}$).